RSC Advances

PAPER

Check for updates

Cite this: *RSC Adv.*, 2022, **12**, 30495

Solvent effects on the motion of a crown ether/amino rotaxane†

Zhen Wu,[a] Shuangshuang Wang,[*ab] Zilin Zhang,[b] Yanjun Zhang,[b] Yanzhen Yin,[*b] Haixin Shi[b] and Shufei Jiao[b]

Solvents have been recognized as a significant factor for modulating the shuttle of rotaxanes and regulating their functions regarding molecular machines by a lot of published studies. The mechanism of the effects of solvents on the motion of crown ether/amino rotaxanes, however, remains unclear. In this work, a rotaxane, formed by dibenzo-24-crown-8 (C[8]) and a dumbbell-shaped axle with two positively charged amino groups, was investigated at the atom level. Two-dimensional free-energy landscapes characterizing the conformational change of C[8] and the shuttling motions in chloroform and water were mapped. The results indicated that the barriers in water were evidently lower than those in chloroform. By analyzing the trajectories, there was no obvious steric effect during shuttling. Instead, the main driving force of shuttling was verified from electrostatic interactions, especially strong hydrogen bonding interactions between the axle and water, which resulted in the fast shuttling rate of the rotaxane. All in all, the polarity and hydrogen bond-forming ability of solvents are the main factors in affecting the shuttling rate of a crown ether/amino rotaxane. In addition, C[8] would adopt S-shaped conformations during shuttling except for situating in the amino sites with C-shaped ones adopted due to π–π stacking interactions. The results of this research improve the comprehension of the solvent modulation ability for shuttling in crown ether-based rotaxanes and illustrate the effects of structural modifications on motions. These new insights are expected to serve the efficient design and construction of molecular machines.

Received 30th August 2022
Accepted 13th October 2022

DOI: 10.1039/d2ra05453a

rsc.li/rsc-advances

1 Introduction

Mechanical interlocked molecular machines are a kind of molecules with some specific functions, which are composed of two or more molecular elements entangled by mechanical bonds in space. As the fundamental archetypes of these molecules, molecular shuttles have attracted increasing public attention due to their diverse functions and great applications such as information storage,[1] molecular logic gates,[2] molecular switches,[3] and medical transportation[4].[5,6] Rotaxanes[7–9] are a typical kind of molecular shuttle and are composed of a linear molecule flanked with stoppers at both termini and a macrocycle threaded onto the latter. The shuttling motion of a rotaxane, namely, the macrocycle in a rotaxane shuttling between two or more sites, could be triggered by assorted external stimuli,[7,10] such as temperature changes,[11,12] pH changes,[13,14] and solvent changes,[15,16] which drive rotaxanes as key factors for the construction of molecular shuttles and motors.[17–19]

Many macrocyclic molecules can be available for the ring components of rotaxanes, for example, crown ethers,[20,21] pillararenes,[11,22] and cyclodextrins[23].[24,25] Crown ethers, as the most flexible macrocyclic molecules,[26] were synthesized and first used as the guest of rotaxanes by Stoddart and coworkers.[27,28] Subsequently, a number of crown ether-based rotaxanes were synthesized and studied such as mushrooms after rain.[29–31] According to these research studies, it was readily found that crown ethers could shuttle between some recognition sites,[32–37] for example, amino groups, benzimidazolium, and bis(pyridinium). Wherein, the molecular machines with the positively charged amino sites attracted more attention. For this kind of molecular machine, the mechanism of movements in rotaxanes and the corresponding driving forces can be summarized as a function of the environment. However, till now, the majority of published studies about crown ether/amino rotaxanes focus on their synthesis and only a small amount of them marginally considered the mechanisms of the movement. In terms of this, Stoddart *et al.* synthesized a molecular shuttle[28] with bis(pyridinium) and amino recognition sites, and found that the shuttle preferred to stay on the positively charged amino sites and could be reversed by a deacidified treatment. Then, Takata *et al.* constructed

[a]*School of Chemistry and Chemical Engineering, Guangxi University, Nanning 530004, China. E-mail: doublewang123@163.com*

[b]*Guangxi Key Laboratory of Green Chemical Materials and Safety Technology, Beibu Gulf University, Qinzhou 535011, China. E-mail: yinyanzhen2009@163.com*

† Electronic supplementary information (ESI) available. See DOI: https://doi.org/10.1039/d2ra05453a

This article is licensed under a Creative Commons Attribution-NonCommercial 3.0 Unported Licence.

(cc) BY-NC

© 2022 The Author(s). Published by the Royal Society of Chemistry

a thermoresponsive rotaxane shuttling system[32] with amino recognition sites, and the resulting molecular machine could be driven by the chemoselective thermal decomposition of ammonium trichloroacetate. Nonetheless, the mechanisms underlying the solvent-controlled behavior of crown ether/amino rotaxanes are still lacking in further studies.

Molecular dynamics simulations (MDS) are a widely used strategy for revealing the internal mechanisms of molecular machines. Cai *et al.*[38] investigated a crown ether-based rotaxane with benzimidazolium and bis(pyridinium) using MDS and indicated that solvents have a significant impact on the shuttling rate. In addition, water could act as lubrication in accelerating the motion of the rotaxane as well. Thus, in this research, all-atom MDS were used for investigating solvent effects on the motion of a crown ether/amino rotaxane. One model of the rotaxane in Fig. 1 was built to compare two solvents, chloroform ($CHCl_3$) and water, which are of great polarity difference. We determined the two-dimensional free-energy landscapes characterizing the shuttling in the rotaxane accompanied by the conformational change of dibenzo-24-crown-8 (C[8]) and then gaged the least free-energy pathways, according to which the most likely conformations of C[8] during shuttling were inferred. By parsing trajectories and dividing the total free energy into physically meaningful individual components, the free-energy contributions extracted from the potentials of means force were analyzed to interpret the driving forces of the shuttling motion and conformational transition. The present work provided a reasonable understanding of the characteristics of driving forces and the mechanisms of the effect of the solvents on the shuttling of crown ether/amino-based rotaxanes. These theoretical findings could be helpful for the rational design of crown ether-based molecular shuttles, which could be controlled by solvents.

2 Simulation details

2.1 Molecular models

The molecular model of a rotaxane formed by a C[8] host and a dumbbell-shaped axle was constructed, as depicted in Fig. 1. The available three-dimensional crystal structure[39] was used for extracting the initial coordinate of C[8]. The molecule assembly was energy-minimized using a conjugate-gradient algorithm and then immersed respectively in a pre-equilibrated box of chloroform and water using the solvate module of the visualization program VMD.[40] For adapting to periodic boundary conditions, any atom of the complex must distance each edge of the boxes from at least 15 Å. Two chloride ions were placed 10 Å away from the rotaxane to ensure electric neutrality in each solvent box. The detail of the molecular assemblies examined in this work is given in Table S1.† Two coarse variables, ξ and d, describing translocation and conformational change of C[8], respectively (defined in Fig. 1B), were chosen to form the transition coordinate. The transition pathways ξ and d were extending from −20 to +20 Å and −3.9 to +3.9 Å, and instantaneous values of both the forces were accrued in bins 0.1 Å wide. The more simulation details can be seen in ESI.†

3 Results and discussion

3.1 Free-energy landscapes underlying the shuttling movement

The two-dimensional free-energy landscapes, characterizing the shuttling motion and conformational change of C[8] along the axle of the rotaxane in $CHCl_3$ and water, are depicted in Fig. 2A

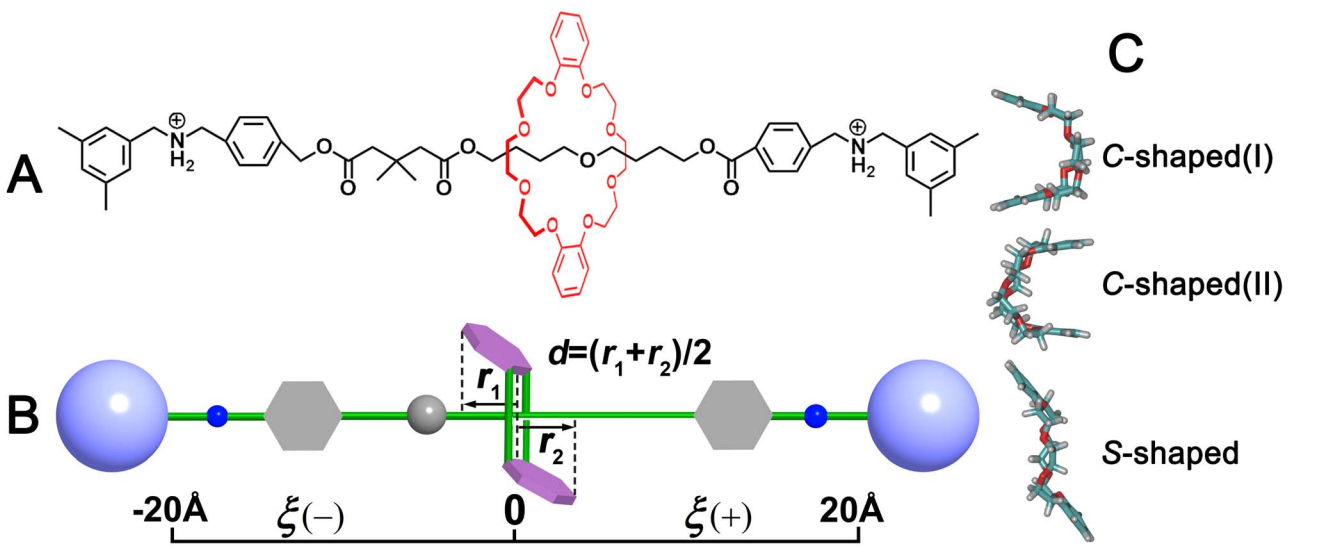

Fig. 1 (A) Chemical structure of the rotaxane formed by C[8] and an axle molecule with two amino recognition sites. (B) Transition coordinates (ξ, d) for free-energy calculations are utilized to explore the putative transition pathways. ξ denotes the projection along the z-direction of the Cartesian space of the vector connecting the centroid of C[8] and that of the axle. r_1 and r_2 are defined as the projection onto the z-axle of the orientation of the benzo groups of C[8]. d was defined as $d = (r_1 + r_2)/2$ to describe the conformational change of C[8]. (C) Two C-shaped conformations were derived from $d = \pm$ 3.0 Å and one S-shaped conformation was derived from $d = 0$ Å.

© 2022 The Author(s). Published by the Royal Society of Chemistry

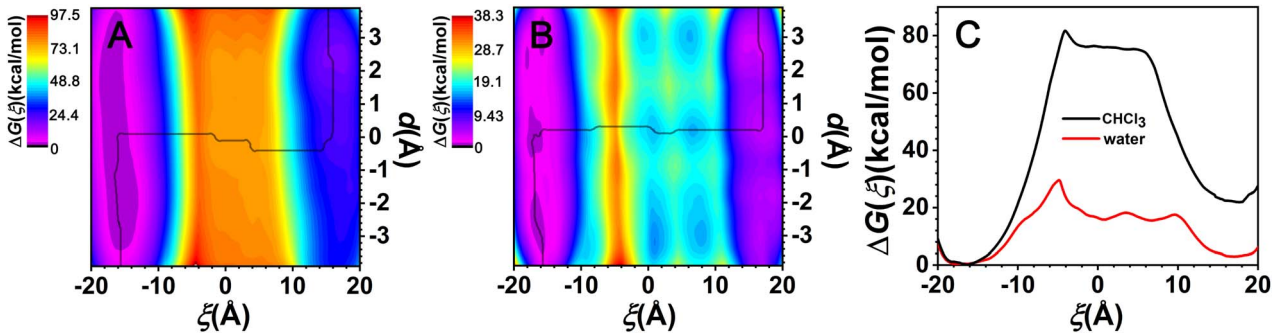

Fig. 2 Free-energy landscapes characterizing the shuttling and conformational change of the rotaxane in $CHCl_3$ (A) and water (B). The black lines show the least free-energy pathways. (C) Free-energy changes for the shuttling movements in two different solvents along ξ according to the least free-energy pathways.

and B. With a cursory glance, these profiles reveal that (i) overall, the barriers of the free-energy landscape in $CHCl_3$ are significantly higher than that in water; (ii) each map features two basins separated by one wide ridge, and the ridge in the free-energy landscape in water is wider than that in $CHCl_3$; and (iii) symmetric basin areas are around $\xi > +10.0$ Å and $\xi < -10.0$ Å for $CHCl_3$ and around $\xi > +12.0$ Å and $\xi < -12.0$ Å for water. The minima of the low-energy areas in the two solvents can be found at $\xi = -16.0$ Å, $d = -2.4$ Å and $\xi = +16.0$ Å, $d = +2.4$ Å, namely, the positively charged amino sites. In the corresponding structures shown in Fig. 3a and c, C[8] adopts C-shaped conformations. The least free-energy pathways connecting these two minima represent the most reasonable transition path for the shuttling of C[8] between two amino sites. It can be seen that C[8] almost adopts S-shaped conformations (see Fig. 3b) during shuttling unless it is located in amino sites.

Fig. 2C shows the one-dimensional free-energy profiles (ODFEs) for shuttling along ξ according to the least free-energy pathways. From the results in $CHCl_3$, the energy barrier to be overcome for shuttling was inferred to be equal to about 81.6 kcal mol^{-1}, while the barrier in water was estimated to be only 29.5 kcal mol^{-1}, thereby indicating that the shuttling rate of the latter is significantly faster than that of the former. Moreover, the two maxima all appear at about $\xi = -4.5$ Å, wherein C[8] overlaps with the neopentane moieties between the two ester groups.

3.2 Free-energy decomposition

According to the above-mentioned analysis, the rotaxane can shuttle between two sites and the shuttling rate is apparently distinct in two solvents. Then, what are the driving forces of the shuttling motion? For this purpose, the free-energy contributions along ξ extracted from the potentials of means force by dividing the total free energy into physically meaningful individual components and binning, averaging, and integrating the force. The results are shown in Fig. 4.

As shown in Fig. 4, the C[8]-axle interactions feature two basins separated by one wide barrier and show similar tendencies as the ODFEs, which indicates that the C[8]-axle interactions constitute the main contributions to the barriers of the ODFEs. The C[8]-axle interactions were further decomposed into van der Waals (C[8]-axle-vdw) and electrostatic (C[8]-axle-elec) contributions. The C[8]-axle-vdw contributions for all solvent conditions generally feature a wide valley, which is because of the suitable size of the C[8] cavity to include the linear molecule. It also illustrates that the solvents have little effects on the C[8]-axle-vdw. It is noteworthy that there is a little bump at about $\xi = -4.5$ Å, which is in agreement with the maxima of the ODFEs. The contribution to the bump is the steric hindrance caused by the neopentane moieties. What is more, the right tail of the C[8]-axle-vdw is higher than the left

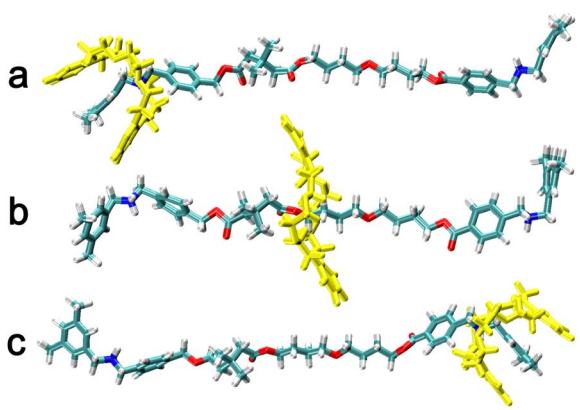

Fig. 3 Representative structures during shuttling. The C[8] is located in (a) and (c) the amino sites and (b) the middle of the axle.

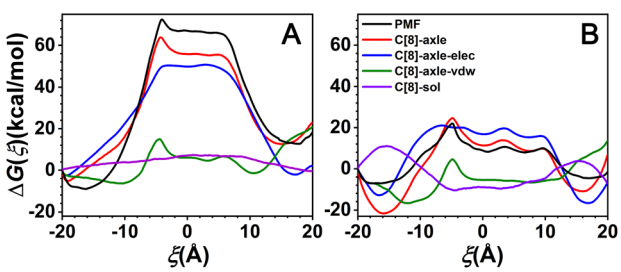

Fig. 4 Breakdown of the total free-energy profiles into C[8]-axle and C[8]-sol contributions, which were further decomposed into electrostatic (C[8]-axle-elec) and van der Waals (C[8]-axle-vdw) contributions, for the shuttling processes of the rotaxane in $CHCl_3$ (A) and water (B). ODFEs are the one-dimensional free-energy profiles for shuttling along ξ.

© 2022 The Author(s). Published by the Royal Society of Chemistry

tail, which could be attributed to the slight asymmetry of the structure, thereby resulting in the asymmetry of the free-energy profiles. The C[8]-axle-elec contributions feature two basins separated by one wide barrier and show similar tendencies as the ODFEs, which illustrates that the electrostatic interactions determine the stable binding sites of C[8] and constitute the main driving force responsible for shuttling. Furthermore, the C[8]-axle-elec in $CHCl_3$ is markedly stronger than that in water, suggesting that the polarity of the solvents has a significant impact on it; the stronger the solvent polarity, the weaker the C[8]-axle-elec. It can be further observed in Fig. 4 that the C[8]-sol contribution in $CHCl_3$ presents a low mound, indicating that it has little effect on the ODFE. By contrast, the C[8]-sol contribution in water possesses two bumps, spanning $\xi \leq -12$ Å and $\xi \geq 12$ Å, separated by a wide and flat domain, implying that while C[8] is located in the amino sites, the C[8]–sol interactions are unfavorable for the shuttling process. Accordingly, the C[8]–sol interactions in the water partly contribute to ODFE.

To appreciate the effect of the solvents on C[8]–sol interactions, the distributions of the solvent molecules around the left amino moiety were monitored. This was achieved by computing the bidimensional radial distribution functions, $g(r; \xi)$, of the C atom of $CHCl_3$ or the O atom of water with respect to the centroid of the selected moieties. The results are gathered in Fig. 5.

As shown in Fig. 5A and B, the maximum density found in the region spanning $5 \leq r \leq 6$ Å in $CHCl_3$ and $3 \leq r \leq 4$ Å in water corresponds to the first solvation shell of the left amino moiety, illustrating that the amino moieties are closer to water molecules than to chloroform molecules. The solvation shell of the left amino moiety is discontinuous along ξ, for $\xi \leq -6$ Å in $CHCl_3$ and $\xi \leq -12$ Å in water, which means that the solvation shell is disrupted as C[8] locates on the amino moiety. With the former moving away from the latter, the solvation shell in water forms faster than that in $CHCl_3$, indicating that water could promote the motion of C[8], namely, that water could act as a lubricant and accelerate the shuttling rate of the rotaxane. According to Fig. 5C, the first solvation shell of C[8], found in the region spanning $4 \leq r \leq 6$ Å, is practically unchanged during shuttling and the density is the highest. However, as shown in Fig. 5D, the density of the solvation shell in water is up to 9.10×10^{-3} and evidently weaker than that in $CHCl_3$, which is up to 0.41. What is more, the density of the first solvation shell in water is the lowest and is slightly weakened as C[8] is located in the amino sites in water. These features illustrate that C[8] has a clear affinity toward $CHCl_3$ and the solvation shell is not affected during shuttling, and instead, the solvation shell can be disrupted because of the weak affinity of C[8] and water.

On balance, both the C[8]-axle and C[8]–sol interactions act on the ODFEs together. Thereinto, the C[8]-axle-elec contributions constitute the main factor for the emergence of the free-energy barriers. The solvent with higher polarity could have a stronger binding ability with the amino moieties, and then weaken the electrostatic interactions between C[8] and the axle, finally accelerating the shuttling rate of the rotaxane. Besides the polarity of the solvents, the hydrogen-bonding (H-bonding) interactions could be one of the main reasons for contributing to the C[8]-axle-elec interactions.

3.3 Analysis of the H-bonding and π–π stacking interactions

The variation in the average number of intermolecular H-bonds formed between the solvents and the axle and between the solvents and the C[8] by analyzing the trajectories is shown in Fig. 6. The H-bonds could be formed between the O atoms of C[8] as acceptors and N–H of the axle as donors. The largest number of the H-bonds between the axle and C[8] is about 1.8 in both solvents, illustrating that the axle will form H-bonds with C[8] with preference to the solvents, while C[8] is located at the amino sites. The difference is that the H-bonds between the axle and C[8] can be maintained when $-18 < \xi < -6$ Å in $CHCl_3$, and only when $-18 < \xi < -12$ Å in water. It indicates that as C[8] moves away from the amino sites, and the H-bonds between the axle and C[8] in water will be released more easily than those in $CHCl_3$. Meanwhile, it can also be found that the number of H-

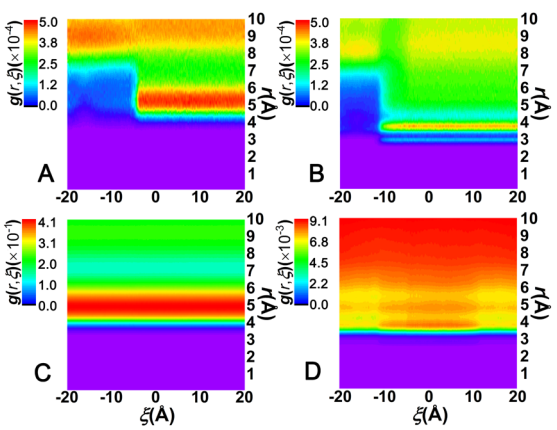

Fig. 5 Variation in the radial distribution function of the center of mass (left amino moiety)-C ($CHCl_3$)/O (water) pair as a function of r, the distance separating the pair of atoms, for the shuttling process (A) in $CHCl_3$, (B) in water. Variation in the radial distribution function of the center of mass (C[8])-C ($CHCl_3$)/O (water) pair as a function of r for the shuttling process (C) in $CHCl_3$ and (D) in water.

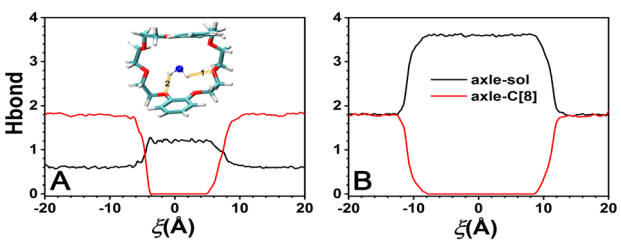

Fig. 6 Variation of the average number of intermolecular H-bonds formed between the axle and the solvents (axle–sol, colored black) and between the axle and the C[8] (axle-C[8], colored red) in $CHCl_3$ (A) and water (B). The inset shows hydrogen bonds formed between the N–H donors of the axle and the acceptor O atoms of the C[8] (N–H···O). The hydrogen-bonding criteria are (i) the angle N–H···O > 135° and (ii) the distance N···O < 3.5 Å. The hydrogen bonds are highlighted in gold.

© 2022 The Author(s). Published by the Royal Society of Chemistry

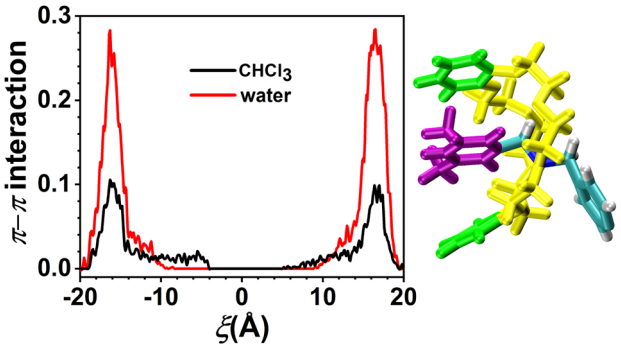

Fig. 7 Variation in the average number of π–π stacking interactions in $CHCl_3$ (colored black) and water (colored red). The π–π stacking criterion is that the distance between the benzene rings of C[8] (colored green) and these of the axle (colored purple) are below 4.

bonds between the axle and solvents increases from 0.6 to 1.2 in $CHCl_3$ and from 1.8 to 3.6 in water, illustrating that the axle can form more H-bonds with water molecules than with $CHCl_3$ molecules. More stable H-bonds between water and the axle impel the H-bonds between C[8] and the axle to be broken earlier and promote the motion of C[8]. Furthermore, the turning points of the curves are consistent with those of the C[8]-axle-elec, illustrating that the H-bonding interactions are one of the main reasons for contributing to the C[8]-axle-elec.

However, according to Fig. 3a and c, C[8] usually adopts C-shaped conformations, while it is near the benzene rings at both ends of the axle. Why? To this end, the π–π stacking interaction, which is a direct attractive non-covalent interaction between aromatic moieties,[41] is considered. The variation in π–π interactions between the axle and C[8] by analyzing the trajectories is shown in Fig. 7. It can be seen that only while C[8] locates at both ends of the axle, π–π stacking interactions are formed between C[8] and the axle. That is to say that C[8] adopts suitable conformations, namely, C-shaped ones, for matching the axle to form the intermolecular forces with the latter, thereby stabilizing the system. The interactions in $CHCl_3$ are stronger than these in water, which illustrates that the stronger the polarity of the solvent is, the stronger the interactions are. However, relative to the H-bonds, π–π stacking interactions are weak and thus make no difference to the ODFE, *i.e.*, the shuttling rate of the rotaxane.

4. Conclusions

Two-dimensional free-energy calculations were utilized for investigating the mechanisms of the crown ether-based rotaxane. The results clearly indicate that the barriers in $CHCl_3$ are significantly higher than those in water and the shuttling of the flexible C[8] along the axle is highly coupled with the conformational transition. The C[8] would adopt an S-shaped conformation during shuttling, unless it could be located in the amino sites with a C-shaped conformation adopted. The main driving force for shuttling is derived from electrostatic interactions between C[8] and the axles by partitioning the free-energy profiles into different components. Both the polarity of the solvents and the capability of H-bonds formation in the solvents have an effect on the barriers and then help to modulate the shuttling of the rotaxane. In detail, the strong solvent polarity can spur C[8] to move away from both the amino moieties and the solvation shell of the latter forms and then activate this motion. Moreover, the H-bonds can show a faster shuttling rate in the solvents due to greater interactions between solvent molecules and the axle due to its release, as C[8] moves away the amino sites. In general, water can act as a lubricant and accelerate the shuttling rate of the rotaxane.

The results in this article introduce a comprehensible solvent modulation ability for shuttling in the crown ether-based rotaxanes and disentangle the effects of the structural modifications on the motions. In the future work, the rotaxanes with crown ether and deprotonated amino sites in several distinguished other solvents will be compared to explore the response mechanisms of the crown ether/amino rotaxanes to environmental change.

Author contributions

Conceptualization, supervision, writing – review and editing, funding acquisition, Shuang-Shuang Wang; data curation, writing – original draft preparation, Zhen Wu and Shuang-Shuang Wang; formal analysis, resources, Yan-Zhen Yin; formal analysis and discussion, Zi-Lin Zhang, and Yan-Jun Zhang; investigation, Hai-Xin Shi and Shu-Fei Jiao. All authors have read and agreed to the published version of the manuscript.

Conflicts of interest

There are no conflicts of interest to declare.

Acknowledgements

This study is supported by Natural Science Foundation of Guangxi Province (No. 2018JJB160116), Marine Science Guangxi First-Class Subject, Beibu Gulf University (No. DTB003).

References

1 A. Coskun, J. M. Spruell, G. Barin, W. R. Dichtel, A. H. Flood, Y. Y. Botros and J. F. Stoddart, *Chem. Soc. Rev.*, 2012, **41**, 4827–4859.
2 Q. Zhang, S. J. Rao, T. Xie, X. Li, T. Y. Xu, D. W. Li, D. H. Qu, Y. T. Long and H. Tian, *Chem*, 2018, **4**, 2670–2684.
3 C. J. Bruns and J. F. Stoddart, *Acc. Chem. Res.*, 2014, **47**, 2186–2199.
4 J. Y. C. Lim, I. Marques, V. Felix and P. D. Beer, *Angew. Chem., Int. Ed.*, 2018, **57**, 584–588.
5 M. W. Ambrogio, C. R. Thomas, Y. L. Zhao, J. I. Zink and J. F. Stoddart, *Acc. Chem. Res.*, 2011, **44**, 903–913.
6 J. J. Yu, Z. Q. Cao, Q. Zhang, S. Yang, D. H. Qu and H. Tian, *Chem. Commun.*, 2016, **52**, 12056–12059.
7 M. Xue, Y. Yang, X. D. Chi, X. Z. Yan and F. H. Huang, *Chem. Rev.*, 2015, **115**, 7398–7501.

© 2022 The Author(s). Published by the Royal Society of Chemistry

8 C. J. Bruns, M. Frasconi, J. Iehl, K. J. Hartlieb, S. T. Schneebeli, C. Cheng, S. I. Stupp and J. F. Stoddart, *J. Am. Chem. Soc.*, 2014, **136**, 4714–4723.

9 J. C. Chang, S. H. Tseng, C. C. Lai, Y. H. Liu, S. M. Peng and S. H. Chiu, *Nat. Chem.*, 2017, **9**, 128–134.

10 H. Li and D. H. Qu, *Sci. China Chem.*, 2015, **58**, 916–921.

11 S. Y. Dong, J. Y. Yuan and F. H. Huang, *Chem. Sci.*, 2014, **5**, 247–252.

12 X. Song, X. F. Zhu, S. Qiu, W. Tian and M. H. Liu, *Angew. Chem., Int. Ed.*, 2022, e202208574.

13 V. Blanco, A. Carlone, K. D. Hänni, D. A. Leigh and B. Lewandowski, *Angew. Chem.*, 2012, **124**, 5256–5259.

14 P. J. Altmann and A. Pöthig, *Angew. Chem., Int. Ed.*, 2017, **56**, 15733–15736.

15 Z. B. Zhang, C. Y. Han, G. C. Yu and F. H. Huang, *Chem. Sci.*, 2012, **3**, 3026–3031.

16 H. H. Fu, X. G. Shao, C. Chipot and W. S. Cai, *Chem. Sci.*, 2017, **8**, 5087–5094.

17 D. H. Qu, Q. C. Wang, Q. W. Zhang, X. Ma and H. Tian, *Chem. Rev.*, 2015, **115**, 7543–7588.

18 S. J. Rao, Q. Zhang, J. Mei, X. H. Ye, C. Gao, Q. C. Wang, D. H. Qu and H. Tian, *Chem. Sci.*, 2017, **8**, 6777–6783.

19 J. S. Cui, Q. K. Ba, H. Ke, A. Valkonen, K. Rissanen and W. Jiang, *Angew. Chem., Int. Ed.*, 2018, **130**, 7935–7940.

20 K. Zhu, V. N. Vukotic, N. Noujeim and S. J. Loeb, *Chem. Sci.*, 2012, **3**, 3265–3271.

21 C. J. Zhang, S. J. Li, J. Q. Zhang, K. L. Zhu, N. Li and F. H. Huang, *Org. Lett.*, 2007, **9**, 5553–5556.

22 M. Xue, Y. Yang, X. D. Chi, Z. Zhang and F. H. Huang, *Acc. Chem. Res.*, 2012, **45**, 1294–1308.

23 C. Casati, P. Franchi, R. Pievo, E. Mezzina and M. Lucarini, *J. Am. Chem. Soc.*, 2012, **134**, 19108–19117.

24 M. Bazzoni, L. Andreoni, S. Silvi, A. Credi, G. Cera, A. Secchi and A. Arduini, *Chem. Sci.*, 2021, **12**, 6419–6428.

25 Y. Han and C. F. Chen, *Acc. Chem. Res.*, 2018, **51**, 2093–2106.

26 S. S. Wang, Y. Z. Yin, J. Gao, X. T Liang and H. X. Shi, *J. Braz. Chem. Soc.*, 2021, **32**, 1963–1971.

27 P. R. Ashton, I. Baxter, M. C. T. Fyfe, F. M. Raymo, N. Spencer, J. F. Stoddart, A. J. P. White and D. J. Williams, *J. Am. Chem. Soc.*, 1998, **120**, 2297–2307.

28 P. R. Ashton, R. Ballardini, V. Balzani, I. Baxter, A. Credi, M. C. T. Fyfe, M. T. Gandolfi, M. Gómez-López, M. Martínez-Díaz, A. Piersanti, N. Spencer, J. F. Stoddart, M. Venturi, A. J. P. White and D. J. Williams, *J. Am. Chem. Soc.*, 1998, **120**, 11932–11942.

29 Z. Meng, J. F. Xiang and C. F. Chen, *J. Am. Chem. Soc.*, 2016, **138**, 5652–5658.

30 R. R. Tao, Q. Zhang, S. J. Rao, X. L. Zheng, M. M. Li and D. H. Qu, *Sci. China: Chem.*, 2019, **62**, 245–250.

31 H. Zhang, X. G. Shao, C. Chipot and W. S. Cai, *J. Phys. Chem. C*, 2019, **123**, 11304–11309.

32 Y. Abe, H. Okamura, K. Nakazono, Y. Koyama, S. Uchida and T. Takata, *Org. Lett.*, 2012, **14**, 4122–4125.

33 S. Corra, C. D. Vet, J. Groppi, M. L. Rosa, S. Silvi, M. Baroncini and A. Credi, *J. Am. Chem. Soc.*, 2019, **141**, 9129–9133.

34 S. J. Cantrill, S. J. Rowan and J. F. Stoddart, *Org. Lett.*, 1999, **1**, 1363–1366.

35 T. Takata, *ACS Cent. Sci.*, 2020, **6**, 129–143.

36 M. Mao, X. K. Zhang, T. Y. Xu, X. D. Wang, S. J. Rao, Y. Liu, D. H. Qu and H. Tian, *Chem. Commun.*, 2019, **55**, 3525–3528.

37 K. L. Zhu, V. N. Vukotic and S. J. Loeb, *Chem.–Asian J.*, 2016, **11**, 3258–3266.

38 S. l. Du, H. H. Fu, X. G. Shao, C. Chipot and W. S. Cai, *J. Phys. Chem. C*, 2018, **122**, 9229–9234.

39 M. Howard, S. M. D. Colquhoun, J. F. Stoddart, A. M. Z. Slawin and D. J. Williams, *J. Chem. Soc., Perkin Trans. 2*, 1986, 253–257.

40 W. Humphrey, A. Dalke and K. Schulten, *J. Mol. Graphics*, 1996, **14**, 33–38.

41 L. J. Riwar, N. Trapp, B. Kuhn and F. Diederich, *Angew. Chem., Int. Ed.*, 2017, **56**, 11252–11257.

© 2022 The Author(s). Published by the Royal Society of Chemistry